Table 2. Associations between patient age and epigenetic features, CIMP and MSI status, and miR-31 expression in serrated lesions according to histopathology

	HPs (n = 142)	p	SSAs (n = 132)	p	TSAs (n = 119)	p
BRAF mutated cases						
Non-elderly	47% (62/132)	0.67	86% (102/119)	0.43	66% (68/103)	0.83
Elderly	40% (4/10)		77% (10/13)		69% (11/16)	
KRAS mutated cases						
Non-elderly	20% (26/130)	0.47	3.4% (4/119)	0.36	20% (20/102)	0.63
Elderly	30% (3/10)		0% (0/13)		25% (4/16)	
IGFBP7 methylated cases						
Non-elderly	13% (17/132)	0.10	38% (45/119)	0.61	17% (17/103)	0.83
Elderly	0% (0/10)		31% (4/13)		19% (3/16)	
MGMT methylated cases						
Non-elderly	3.9% (5/129)	0.42	8.4% (10/119)	0.14	8.8% (9/102)	0.098
Elderly	10% (1/10)		23% (3/13)		0% (0/16)	
MLH1 methylated cases						
Non-elderly	3.1% (4/129)	0.34	18% (21/119)	0.027	3% (3/101)	0.34
Elderly	10% (1/10)		46% (6/13)		0% (0/16)	
RASSF2 methylated cases						
Non-elderly	3.8% (5/132)	0.39	18% (21/119)	0.28	14% (14/103)	0.60
Elderly	0% (0/10)		31% (4/13)		19% (3/16)	
CIMP-high cases						
Non-elderly	7.8% (10/129)	0.24	41% (49/119)	0.38	19% (19/102)	0.27
Elderly	20% (2/10)		54% (7/13)		31% (5/16)	
MSI-high cases						
Non-elderly	1.5% (2/132)	0.59	1.7% (2/119)	0.0042	2% (2/102)	0.38
Elderly	0% (0/10)		23% (3/13)		6.3% (1/16)	
High miR-31 cases						
Non-elderly	16% (21/132)	0.74	36% (43/119)	0.022	43% (43/100)	0.37
Elderly	20% (2/10)		69% (9/13)		31% (5/16)	

Percentages indicate the proportion of patients based on age (non-elderly, aged <75 years; elderly, aged ≥75 years) according to histopathology.

tients (36, 33, 4.3 and 9.2%, respectively, aged <75 years, all $p < 0.01$). No significant differences were found between elderly CRC patients and younger patients for other clinical and molecular features. Based on Kaplan-Meier analysis, older age (elderly) was not significantly associated with patient survival for CRC-specific mortality (data not shown).

Discussion

We conducted this study to identify the clinical, pathological and molecular features of colorectal tumors found in elderly Japanese patients. The frequency of elderly patients with SSAs with cytological dysplasia was significantly higher than that of those with other serrated lesions and non-serrated adenomas. In elderly patients, all SSAs were located in the proximal colon. With regard to molecular alterations, high miR-31 expression, *MLH1* methylation and MSI-high status were more frequently detected in SSAs from elderly patients than in those from non-elderly patients. In contrast, no significant differences were found between older age of onset and HGD for TSAs or non-serrated adenomas in any of these molecular alterations.

A number of investigators have reported that SSAs with cytological dysplasia have genetic and epigenetic abnormalities and are at a high risk of progression to CRCs [10, 12, 16–18, 26, 32]. *MLH1* methylation leads to MSI-high CRC, and repeat tract mutations in genes such as *TGFβRII* are restricted to those lesions with cytological dysplasia in SSAs [26, 33–35]. We recently reported that

the frequency of CIMP-high status was much higher in SSAs with cytological dysplasia than in those without dysplasia [17]. Moreover, our current data showed that *MLH1* methylation and MSI-high status were more frequently detected in SSAs from elderly patients than in those from non-elderly patients. These results suggest that *MLH1* methylation that leads to MSI-high CRC may accumulate with aging and play an important role in SSA progression.

MicroRNAs (miRNAs) are a class of small non-coding RNA molecules that act as posttranscriptional gene regulators and have been increasingly recognized as useful biomarkers for CRC [1, 17]. Using microRNA array analysis, we recently discovered that miR-31 expression was significantly upregulated in *BRAF*-mutated CRCs compared with that in wild-type CRCs [1]. Moreover, associations were found between miR-31 expression, proximal tumor location and poor CRC prognosis. We also reported that the frequency of high miR-31 expression was higher in SSAs with cytological dysplasia than that in SSAs without dysplasia [17]. In the current study, our data showed that the frequency of high miR-31 expression was significantly higher in SSAs from elderly patients than in those from non-elderly patients. Because no previous study has reported on an association between the age of onset and miRNA expression in colorectal serrated lesions, this is the first report to show that miR-31 may be an age-dependent factor for SSA.

Previous studies conducted in the USA and European countries reported that the frequencies of being female, proximal colon location, *BRAF* mutations and CIMP-high status were significantly higher for elderly CRC patients than for non-elderly patients [22, 27–29]. Similar results were observed in the current study using a large number of samples from Japanese CRC patients. This suggests that there are no differences in the clinical and molecular features between elderly Japanese and Caucasian patients with CRC.

In conclusion, in elderly patients, all SSAs were located in the proximal colon. Furthermore, cytological dysplasia was more frequently detected in elderly patients with SSAs than in non-elderly patients. High miR-31 expression, *MLH1* methylation and MSI-high status were more frequently detected in SSAs from elderly patients than in those from non-elderly patients, suggesting that in SSAs these molecular alterations may accumulate with aging. Therefore, these findings indicate that a careful colonoscopic examination of the proximal colon (particularly the cecum to ascending colon) is necessary for elderly patients because SSAs in these patients may exhibit a malignant potential.

Acknowledgements

We thank the pathology departments of Sapporo Medical University Hospital, Keiyukai Sapporo Hospital and JR Sapporo Hospital for providing the tissue specimens.

This work was supported by the Japan Society for the Promotion of Science (JSPS) Grant-in-Aid for Scientific Research (grant No. 23790800), Ono Cancer Research Fund, Suhara Memorial Foundation, Takeda Science Foundation, and Yuasa Memorial Foundation. The authors would like to thank Enago (www.enago.jp) for the English language review.

Disclosure Statement

No conflict of interest.

References

1 Nosho K, Igarashi H, Nojima M, Ito M, Maruyama R, Yoshii S, Naito T, Sukawa Y, Mikami M, Sumioka W, Yamamoto E, Kurokawa S, Adachi Y, Takahashi H, Okuda H, Kusumi T, Hosokawa M, Fujita M, Hasegawa T, Okita K, Hirata K, Suzuki H, Yamamoto H, Shinomura Y: Association of microRNA-31 with BRAF mutation, colorectal cancer survival and serrated pathway. Carcinogenesis 2014;35:776–783.

2 Ogino S, Nosho K, Kirkner GJ, Kawasaki T, Meyerhardt JA, Loda M, Giovannucci EL, Fuchs CS: CpG island methylator phenotype, microsatellite instability, BRAF mutation and clinical outcome in colon cancer. Gut 2009;58:90–96.

3 Okada Y, Miyamoto H, Goji T, Takayama T: Biomarkers for predicting the efficacy of anti-epidermal growth factor receptor antibody in the treatment of colorectal cancer. Digestion 2014;89:18–23.

4 Bentz S, Cee A, Endlicher E, Wojtal KA, Naami A, Pesch T, Lang S, Schubert P, Fried M, Weber A, Coy JF, Goelder S, Knuchel R, Hausmann M, Rogler G: Hypoxia induces the expression of transketolase-like 1 in human colorectal cancer. Digestion 2013;88:182–192.

5 Laiyemo AO, Doubeni C, Pinsky PF, Doria-Rose VP, Marcus PM, Schoen RE, Lanza E, Cross AJ: Factors associated with the risk of adenoma recurrence in distal and proximal colon. Digestion 2013;87:141–146.

6 Liao X, Lochhead P, Nishihara R, Morikawa T, Kuchiba A, Yamauchi M, Imamura Y, Qian ZR, Baba Y, Shima K, Sun R, Nosho K, Meyerhardt JA, Giovannucci E, Fuchs CS, Chan AT, Ogino S: Aspirin use, tumor PIK3CA mutation, and colorectal-cancer survival. N Engl J Med 2012;367:1596–1606.

7 Nosho K, Kure S, Irahara N, Shima K, Baba Y, Spiegelman D, Meyerhardt JA, Giovannucci EL, Fuchs CS, Ogino S: A prospective cohort study shows unique epigenetic, genetic, and prognostic features of synchronous colorectal cancers. Gastroenterology 2009;137:1609–1620.e3.

8 Edelstein DL, Axilbund JE, Hylind LM, Romans K, Griffin CA, Cruz-Correa M, Giardiello FM: Serrated polyposis: rapid and relentless development of colorectal neoplasia. Gut 2013;62:404–408.
9 Rosty C, Buchanan DD, Walsh MD, Pearson SA, Pavluk E, Walters RJ, Clendenning M, Spring KJ, Jenkins MA, Win AK, Hopper JL, Sweet K, Frankel WL, Aronson M, Gallinger S, Goldblatt J, Woodall S, Arnold J, Walker NI, Jass JR, Parry S, Young JP: Phenotype and polyp landscape in serrated polyposis syndrome: a series of 100 patients from genetics clinics. Am J Surg Pathol 2012;36:876–882.
10 Rex DK, Ahnen DJ, Baron JA, Batts KP, Burke CA, Burt RW, Goldblum JR, Guillem JG, Kahi CJ, Kalady MF, O'Brien MJ, Odze RD, Ogino S, Parry S, Snover DC, Torlakovic EE, Wise PE, Young J, Church J: Serrated lesions of the colorectum: review and recommendations from an expert panel. Am J Gastroenterol 2012;107:1315–1330.
11 Burnett-Hartman AN, Newcomb PA, Potter JD, Passarelli MN, Phipps AI, Wurscher MA, Grady WM, Zhu LC, Upton MP, Makar KW: Genomic aberrations occurring in subsets of serrated colorectal lesions but not conventional adenomas. Cancer Res 2013;73:2863–2872.
12 Fujita K, Yamamoto H, Matsumoto T, Hirahashi M, Gushima M, Kishimoto J, Nishiyama K, Taguchi T, Yao T, Oda Y: Sessile serrated adenoma with early neoplastic progression: a clinicopathologic and molecular study. Am J Surg Pathol 2011;35:295–304.
13 Fu B, Yachida S, Morgan R, Zhong Y, Montgomery EA, Iacobuzio-Donahue CA: Clinicopathologic and genetic characterization of traditional serrated adenomas of the colon. Am J Clin Pathol 2012;138:356–366.
14 Mohammadi M, Kristensen MH, Nielsen HJ, Bonde JH, Holck S: Qualities of sessile serrated adenoma/polyp/lesion and its borderline variant in the context of synchronous colorectal carcinoma. J Clin Pathol 2012;65:924–927.
15 Kaji E, Uraoka T, Kato J, Hiraoka S, Suzuki H, Akita M, Saito S, Tanaka T, Ohara N, Yamamoto K: Externalization of saw-tooth architecture in small serrated polyps implies the presence of methylation of IGFBP7. Dig Dis Sci 2012;57:1261–1270.
16 Rosty C, Hewett DG, Brown IS, Leggett BA, Whitehall VL: Serrated polyps of the large intestine: current understanding of diagnosis, pathogenesis, and clinical management. J Gastroenterol 2013;48:287–302.
17 Ito M, Mitsuhashi K, Igarashi H, Nosho K, Naito T, Yoshii S, Takahashi H, Fujita M, Sukawa Y, Yamamoto E, Takahashi T, Adachi Y, Nojima M, Sasaki Y, Tokino T, Baba Y, Maruyama R, Suzuki H, Imai K, Yamamoto H, Shinomura Y: MicroRNA-31 expression in relation to BRAF mutation, CpG island methylation and colorectal continuum in serrated lesions. Int J Cancer 2014;135:2507–2515.
18 Naito T, Nosho K, Ito M, Igarashi H, Mitsuhashi K, Yoshii S, Aoki H, Nomura M, Sukawa Y, Yamamoto E, Adachi Y, Takahashi H, Hosokawa M, Fujita M, Takenouchi T, Maruyama R, Suzuki H, Baba Y, Imai K, Yamamoto H, Ogino S, Shinomura Y: IGF2 DMR hypomethylation in relation to pathological and molecular features of serrated lesions. World J Gastroenterol 2014;20:10050–10061.
19 Dhir M, Yachida S, van Neste L, Glockner SC, Jeschke J, Pappou EP, Montgomery EA, Herman JG, Baylin SB, Iacobuzio-Donahue C, Ahuja N: Sessile serrated adenomas and classical adenomas: an epigenetic perspective on premalignant neoplastic lesions of the gastrointestinal tract. Int J Cancer 2011;129:1889–1898.
20 Toyota M, Ahuja N, Ohe-Toyota M, Herman JG, Baylin SB, Issa JP: CpG island methylator phenotype in colorectal cancer. Proc Natl Acad Sci USA 1999;96:8681–8686.
21 Weisenberger DJ, Siegmund KD, Campan M, Young J, Long TI, Faasse MA, Kang GH, Widschwendter M, Weener D, Buchanan D, Koh H, Simms L, Barker M, Leggett B, Levine J, Kim M, French AJ, Thibodeau SN, Jass J, Haile R, Laird PW: CpG island methylator phenotype underlies sporadic microsatellite instability and is tightly associated with BRAF mutation in colorectal cancer. Nat Genet 2006;38:787–793.
22 Yamauchi M, Morikawa T, Kuchiba A, Imamura Y, Qian ZR, Nishihara R, Liao X, Waldron L, Hoshida Y, Huttenhower C, Chan AT, Giovannucci E, Fuchs C, Ogino S: Assessment of colorectal cancer molecular features along bowel subsites challenges the conception of distinct dichotomy of proximal versus distal colorectum. Gut 2012;61:847–854.
23 Nosho K, Irahara N, Shima K, Kure S, Kirkner GJ, Schernhammer ES, Hazra A, Hunter DJ, Quackenbush J, Spiegelman D, Giovannucci EL, Fuchs CS, Ogino S: Comprehensive biostatistical analysis of CpG island methylator phenotype in colorectal cancer using a large population-based sample. PLoS One 2008;3:e3698.
24 Donehower LA, Creighton CJ, Schultz N, Shinbrot E, Chang K, Gunaratne PH, Muzny D, Sander C, Hamilton SR, Gibbs RA, Wheeler D: MLH1-silenced and non-silenced subgroups of hypermutated colorectal carcinomas have distinct mutational landscapes. J Pathol 2013;229:99–110.
25 Leggett B, Whitehall V: Role of the serrated pathway in colorectal cancer pathogenesis. Gastroenterology 2010;138:2088–2100.
26 Bettington M, Walker N, Clouston A, Brown I, Leggett B, Whitehall V: The serrated pathway to colorectal carcinoma: current concepts and challenges. Histopathology 2013;62:367–386.
27 Lochhead P, Kuchiba A, Imamura Y, Liao X, Yamauchi M, Nishihara R, Qian ZR, Morikawa T, Shen J, Meyerhardt JA, Fuchs CS, Ogino S: Microsatellite instability and BRAF mutation testing in colorectal cancer prognostication. J Natl Cancer Inst 2013;105:1151–1156.
28 Perea J, Rueda D, Canal A, Rodriguez Y, Alvaro E, Osorio I, Alegre C, Rivera B, Martinez J, Benitez J, Urioste M: Age at onset should be a major criterion for subclassification of colorectal cancer. J Mol Diagn 2014;16:116–126.
29 Chen D, Huang JF, Liu K, Zhang LQ, Yang Z, Chuai ZR, Wang YX, Shi DC, Huang Q, Fu WL: BRAFV600E mutation and its association with clinicopathological features of colorectal cancer: a systematic review and meta-analysis. PLoS One 2014;9:e90607.
30 Nosho K, Yamamoto H, Takahashi T, Mikami M, Taniguchi H, Miyamoto N, Adachi Y, Arimura Y, Itoh F, Imai K, Shinomura Y: Genetic and epigenetic profiling in early colorectal tumors and prediction of invasive potential in pT1 (early invasive) colorectal cancers. Carcinogenesis 2007;28:1364–1370.
31 Suzuki H, Igarashi S, Nojima M, Maruyama R, Yamamoto E, Kai M, Akashi H, Watanabe Y, Yamamoto H, Sasaki Y, Itoh F, Imai K, Sugai T, Shen L, Issa JP, Shinomura Y, Tokino T, Toyota M: IGFBP7 is a p53-responsive gene specifically silenced in colorectal cancer with CpG island methylator phenotype. Carcinogenesis 2010;31:342–349.
32 Yamamoto E, Suzuki H, Yamano HO, Maruyama R, Nojima M, Kamimae S, Sawada T, Ashida M, Yoshikawa K, Kimura T, Takagi R, Harada T, Suzuki R, Sato A, Kai M, Sasaki Y, Tokino T, Sugai T, Imai K, Shinomura Y, Toyota M: Molecular dissection of premalignant colorectal lesions reveals early onset of the CpG island methylator phenotype. Am J Pathol 2012;181:1847–1861.
33 Ricciardiello L, Goel A, Mantovani V, Fiorini T, Fossi S, Chang DK, Lunedei V, Pozzato P, Zagari RM, De Luca L, Fuccio L, Martinelli GN, Roda E, Boland CR, Bazzoli F: Frequent loss of hMLH1 by promoter hypermethylation leads to microsatellite instability in adenomatous polyps of patients with a single first-degree member affected by colon cancer. Cancer Res 2003;63:787–792.
34 Cunningham JM, Christensen ER, Tester DJ, Kim CY, Roche PC, Burgart LJ, Thibodeau SN: Hypermethylation of the hMLH1 promoter in colon cancer with microsatellite instability. Cancer Res 1998;58:3455–3460.
35 Sheridan TB, Fenton H, Lewin MR, Burkart AL, Iacobuzio-Donahue CA, Frankel WL, Montgomery E: Sessile serrated adenomas with low- and high-grade dysplasia and early carcinomas: an immunohistochemical study of serrated lesions 'caught in the act'. Am J Clin Pathol 2006;126:564–571.

RHEUMATOLOGY

Rheumatology 2015;54:45–49
doi:10.1093/rheumatology/keu228
Advance Access publication 6 June 2014

Concise report

Identification of relapse predictors in IgG4-related disease using multivariate analysis of clinical data at the first visit and initial treatment

Motohisa Yamamoto[1], Masanori Nojima[2], Hiroki Takahashi[1], Yoshihiro Yokoyama[1], Keisuke Ishigami[1], Hidetaka Yajima[1], Yui Shimizu[1], Tetsuya Tabeya[1], Mikiko Matsui[1], Chisako Suzuki[1], Yasuyoshi Naishiro[1], Ken-ichi Takano[3], Tetsuo Himi[3], Kohzoh Imai[4] and Yasuhisa Shinomura[1]

Abstract

Objectives. Inducting clinical remission by glucocorticoid treatment is relatively easy in IgG4-related disease (IgG4-RD), but relapse also occurs easily with tapering of the steroid dose. The present study tried to analyse the cases to extract predictors of relapse present at the diagnosis of IgG4-RD.

Methods. Subjects comprised 79 patients with IgG4-related dacryoadenitis and sialadenitis, known as Mikulicz's disease, who were diagnosed between April 1997 and October 2013 and followed-up for >2 years from the initial induction treatment. They were applied to Cox proportional hazard modelling, based on the outcome of interval to relapse. We performed multivariate analysis for the clinical factors of these cases and identified predictors of relapse.

Results. Identified factors were male sex and younger onset in cases without organ involvement at diagnosis and low levels of serum IgG4 in cases with organ dysfunction at diagnosis. Complication with autoimmune pancreatitis and low steroid dose at initial treatment also tended to be associated with recurrence.

Conclusion. Follow-up is important in cases with recognized risk factors for relapse, including male sex and younger onset in cases without organ damage.

Key words: autoimmune pancreatitis, IgG4-related disease, Mikulicz's disease, multivariate analysis, relapse.

Introduction

IgG4-related disease (IgG4-RD) can cause irreversible damage to various organs through type 2 T helper (Th2) inflammation and progressive fibrosis [1, 2]. Induction of clinical remission is easily achieved using glucocorticoid treatment [3], but relapse also readily occurs when the steroid dose is tapered [4]. The annual rate of recurrence in 2012 was 19.0% in our facility, and half of relapsed cases reportedly present with new organ lesions [5]. On the other hand, many cases can continue in clinical remission with low-dose glucocorticoid, and steroid can even be discontinued in some cases. Because no markers can reflect disease activity and predict relapse in IgG4-RD, rheumatologists often encounter difficulties in clinical practice. Thus the present study tried to analyse cases followed for >2 years after initiating therapy to extract predictors of relapse present at the diagnosis of IgG4-RD.

Methods

Subjects comprised 79 patients with IgG4-related dacryoadenitis and sialadenitis, known as Mikulicz's

[1]Department of Gastroenterology, Rheumatology and Clinical Immunology, Sapporo Medical University School of Medicine, Sapporo, [2]Division of Advanced Medicine Promotion, Advanced Clinical Research Center, Institute of Medical Science, University of Tokyo, Tokyo, [3]Department of Otolaryngology, Sapporo Medical University School of Medicine, Sapporo and [4]Center for Antibody and Vaccine Therapy, Institute of Medical Science, University of Tokyo, Tokyo, Japan

Submitted 15 December 2013; revised version accepted 1 April 2014.

Correspondence to: Motohisa Yamamoto, Department of Gastroenterology, Rheumatology and Clinical Immunology, Sapporo Medical University School of Medicine, South 1, West 16, Chuo-ku, Sapporo, Hokkaido 0608543 Japan. E-mail: mocha@cocoa.plala.or.jp

CLINICAL SCIENCE

disease, who were diagnosed between April 1997 and October 2013 and followed up for >2 years from the initial induction treatment. Cases were diagnosed with bilateral and continuous enlargement of the lacrimal and salivary glands, elevated levels of serum IgG4 and abundant infiltration of IgG4-bearing plasmacytes into involved organs. We analysed the following clinical factors: sex; age at onset; disease duration; eosinophil count; serum levels of IgG, IgG4 and IgE at diagnosis; presence of hypocomplementaemia and ANA and levels of RF at diagnosis; presence of organ involvement other than the lacrimal and salivary glands; numbers of organ lesions other than those of the lacrimal and salivary glands; complication with autoimmune pancreatitis, IgG4-related kidney disease or retroperitoneal fibrosis and the initial dose of steroid. Disease duration was defined as the interval between the appearance of subjective symptoms and the start of treatment. Autoimmune pancreatitis, IgG4-related kidney disease and retroperitoneal fibrosis were diagnosed based on imaging findings. As our treatment protocol, starting prednisolone at a dose of 0.6 mg/kg/day was appropriate with only lacrimal and salivary gland involvement, increasing to 1.0 mg/kg/day with multiple organ lesions. The initial dose of prednisolone was continued for 2–4 weeks, tapering the dose by 10% every 2 weeks. If the patient was >80 years of age or had existing complications, the amount of prednisolone was decreased up to 30% of the predetermined amount. Relapse was defined as re-enlargement of the lacrimal and/or salivary glands or appearance of other organ involvement.

First, all 79 cases were applied to Cox proportional hazard modelling, based on the outcome of interval to relapse. We performed uni- and multivariate analysis for each clinical factor and identified predictors of relapse. On multivariate analysis, we used the backward elimination method (Wald method, excluding factors presenting with $P > 0.1$) and extracted the factors offering high predictive power. The existence of organ involvement was considered to represent a strong risk factor for relapse. We stratified patients into groups with and without organ lesions at diagnosis and performed uni- and multivariate analysis for each group. In multivariate analysis, we applied those variables that showed $P < 0.2$ in univariate analysis and used the backward elimination method (Wald method, excluding factors presenting with $P > 0.1$). P-values < 0.05 were considered statistically significant. All statistical analyses were performed using SPSS Statistics version 20.0.0 software (IBM, Armonk, NY, USA).

Written consent to use the information from these cases was obtained from all patients in accordance with the Declaration of Helsinki. This study proceeded under the approval of the Sapporo Medical University Hospital Institutional Review Board (SMU 22-57, 24-155).

Results

Table 1 shows the profiles of the patients. For the 79 cases, age at onset, presence of organ involvement and complication of autoimmune pancreatitis at diagnosis in univariate analysis and age at onset, levels of serum IgG and RF and presence of organ involvement at diagnosis in multivariate analysis were extracted.

The results from analyses by group with and without organ involvement, which was considered a strong predictor of relapse, showed that sex, age at onset and disease duration were significant on univariate analysis and sex and age at onset were extracted from multivariate analysis for the group without organ lesions at diagnosis. On the other hand, levels of serum IgG and IgG4 at diagnosis were significant on univariate analysis and the level of serum IgG at diagnosis was extracted by multivariate analysis for the group with organ dysfunction (Table 2).

TABLE 1 Characteristics of the patients

	Organ involvement at the first visit			
	Presence		Absence	
	No relapse during follow-up *n* = 28	Relapse during follow-up *n* = 5	No relapse during follow-up *n* = 24	Relapse during follow-up *n* = 22
Male:female, mean (S.D.)	8:20 (1:2.5)	3:2 (1:0.7)	16:8 (1:0.5)	10:12 (1:1.2)
Age at onset, mean (S.D.), years	62.6 (10.8)	45.8 (18.0)	60.3 (8.5)	55.2 (12.7)
Period of illness, mean (S.D.), years	1.39 (1.69)	4.00 (3.39)	1.29 (1.81)	2.45 (2.63)
Eosinophils, mean (S.D.), per ml	220.7 (252.8)	106.0 (60.7)	234.4 (195.5)	314.3 (287.8)
Serum IgG, mean (S.D.), mg/dl	2035.0 (1027.0)	1479.6 (160.2)	3326.3 (2338.5)	2264.5 (880.4)
Serum IgG4, mean (S.D.), mg/dl	556.5 (393.2)	221.8 (181.1)	1192.1 (1033.4)	716.7 (466.8)
Serum IgE, mean (S.D.), IU/ml	314.1 (439.4)	412.4 (395.5)	470.8 (391.9)	272.1 (241.3)
Hypocomplementaemia, %	14.3	20.0	29.2	18.2
ANA positive, %	17.9	40.0	25.0	18.2
RF positive, %	14.3	60.0	16.7	18.2

TABLE 2 Uni- and multivariate analysis for risk factors associated with relapse in IgG4-related disease

	Univariate analysis			Multivariate analysis		
	P-value	Hazard ratio	95% CI	*P*-value	Hazard ratio	95% CI
Totals ($n = 79$)						
Male sex	0.120	1.869	0.850, 4.109			
Age at onset	**0.006**	**0.961**	0.935, 0.989	**0.004**	**0.955**	0.925, 0.985
Disease duration	0.062	1.119	0.994, 1.261			
Eosinophil count	0.641	1.000	0.998, 1.001			
Serum level of IgG before Tx	0.052	1.000	0.999, 1.000	**0.003**	**0.999**	0.999, 1.000
Serum level of IgG4 before Tx	0.111	0.999	0.999, 1.000			
Serum level of IgE before Tx	0.180	0.999	0.998, 1.000	0.051	0.999	0.997, 1.000
Hypocomplementaemia	0.312	0.602	0.225, 1.612			
ANA	0.707	0.839	0.337, 2.093			
RF	0.575	1.281	0.540, 3.042			
RF titre	0.743	0.998	0.989, 1.008	**0.010**	**1.018**	1.004, 1.033
Other organ involvement	**0.010**	**3.590**	1.355, 9.512	**<0.001**	**11.077**	3.028, 40.523
Number of other organ involvements	0.122	1.340	0.925, 1.940			
Autoimmune pancreatitis	**0.013**	**3.184**	1.280, 7.924			
IgG4-related kidney disease	0.953	0.968	0.333, 2.813			
Retroperitoneal fibrosis	0.447	1.379	0.603, 3.151			
Initial dose of glucocorticoid	0.595	1.009	0.977, 1.041	0.050	0.953	0.908, 1.000
Without organ involvement ($n = 33$)						
Male sex	0.078	7.842	0.796, 77.228	**0.015**	**342.461**	3.069, 38217.013
Age at onset	**0.022**	**0.938**	0.887, 0.991	**0.004**	**0.856**	0.769, 0.952
Disease duration	**0.008**	**1.554**	1.122, 2.152			
Eosinophil count	0.215	0.994	0.984, 1.004			
Serum level of IgG before Tx	0.115	0.996	0.992, 1.001			
Serum level of IgG4 before Tx	0.116	0.995	0.989, 1.001			
Serum level of IgE before Tx	0.996	1.000	0.998, 1.002			
Hypocomplementaemia	0.958	0.941	0.102, 8.715			
ANA	0.231	3.015	0.496, 18.334			
RF	0.108	4.397	0.724, 26.721			
RF titre	0.881	0.998	0.967, 1.029			
Initial dose of glucocorticoid	0.320	1.094	0.916, 1.306			
With organ involvement ($n = 46$)						
Male sex	0.928	1.041	0.441, 2.453			
Age at onset	0.152	0.974	0.939, 1.010			
Disease duration	0.882	1.011	0.875, 1.168			
Eosinophil count	0.978	1.000	0.998, 1.002			
Serum level of IgG before Tx	**0.012**	**0.999**	0.999, 1.000	**0.015**	**0.999**	(0.999, 1.000)
Serum level of IgG4 before Tx	**0.023**	**0.999**	0.999, 1.000			
Serum level of IgE before Tx	0.142	0.999	0.997, 1.000			
Hypocomplementaemia	0.204	0.491	0.164, 1.472			
ANA	0.148	0.438	0.144, 1.338			
RF	0.933	0.954	0.319, 2.851			
RF titre	0.800	0.999	0.990, 1.007			
Number of other organ involvements	0.375	0.732	0.367, 1.459			
Autoimmune pancreatitis	0.089	2.417	0.875, 6.673	0.054	2.828	(0.981, 8.157)
IgG4-related kidney disease	0.337	0.587	0.198, 1.741			
Retroperitoneal fibrosis	0.553	0.767	0.320, 1.842			
Initial dose of glucocorticoid	0.127	0.974	0.941, 1.008	0.055	0.960	0.921, 1.001

Tx: treatment. Significant values are indicated in bold. The upper section of the table shows total, the middle section shows without organ involvement other than lacrimal and salivary gland lesions and the lower section shows with organ involvement other than lacrimal and salivary gland lesions.

Male sex and younger onset in cases without organ involvement and a low level of serum IgG at diagnosis in cases with organ dysfunction were identified as predictors of relapse.

Discussion

The results of this analysis showed that extracted predictors of relapse differed between cases with

and without organ dysfunction at diagnosis in IgG4-related dacryoadenitis and sialadenitis. This might provide an opportunity to reconsider initial treatment in IgG4-RD.

First, we discuss cases without organ lesions other than of the lacrimal and salivary glands in IgG4-related dacryoadenitis and sialadenitis. Male sex and younger onset were predictors of relapse. IgG4-RD is a disorder based on Th2 inflammation [1]. With regard to the relationship between Th1/Th2 cytokine balance and sex hormones, oestrogen is known to promote the Th1 response [6], while progesterone promotes Th2 inflammation [7]. For this reason we have sometimes found that symptoms worsen when a female patient with IgG4-RD becomes pregnant. In addition, Th1 response is gradually suppressed in menopause due to the reduction in the production of oestrogen. In other words, Th2 immune response tends to be dominant in women after menopause. On the other hand, dihydrotestosterone, an active androgen, inhibits both Th1 and Th2 immune responses [8]. Th2 response is less likely to arise in males and younger patients due to the sex hormone environment. The occurrence of IgG4-RD in males and younger patients may thus suggest high disease activity. These results could also be confirmed using the SMART (Sapporo Medical University and related institutes database for investigation and best treatments of IgG4-RD) cohort database. We analysed 110 cases treated with maintenance therapy and overlapped them with the 79 subjects in the main analysis. The annual relapse rate in the male cases without organ involvement was 9.09% and in the female cases it was 3.85%. The amount of prednisolone at the maintenance treatment was 5.27 mg/day (S.D. 2.72) in males without organ involvement and 3.96 mg/day (S.D. 2.82) in females. Furthermore, there was no relapse in patients who were $\geqslant$70 years of age.

On the other hand, the low levels of serum IgG before treatment in cases with organ dysfunction are difficult to interpret. It was previously reported that expression levels of IL-6 mRNA at diagnosis of IgG4-RD were not significantly low [9]. The interpretation of this result is very difficult at present. In our analysis, complication with autoimmune pancreatitis and the use of low-dose glucocorticoid at initial induction therapy were not significant factors, but tended to be associated with relapse in cases with organ involvement. These factors might be identified as significant with increased numbers of cases for analysis.

The rate of complication with autoimmune pancreatitis was approximately 20% in these patients. Although this study could not suggest a precise interpretation, there was also a high rate of relapse in younger cases with autoimmune pancreatitis. This subject was not included in the cases with only autoimmune pancreatitis, and so was not statistically examined, but younger and male might be predictive risk factors in IgG4-RD.

There is currently no guideline on treatment in IgG4-RD as a whole. Japanese pancreatologists have developed a treatment guideline only for autoimmune pancreatitis. It recommends that the indication for steroid treatment is only symptomatic, starting at 0.6 mg/kg/day of prednisolone as initial dose [10]. This strategy can lead to clinical remission, but relapse often occurs. It is possible that the initial dose, which is required for the pathogenesis, is insufficient. Our analysis showed that the rate of recurrence was high in cases where we could not prescribe the predetermined amount and cases with multiple organ involvement.

We also have to follow up those cases with recognized risk factors for relapse, namely male sex and younger onset in the absence of organ damage. A sufficient dose of steroid at the initial induction treatment may inhibit recurrence in cases complicated with autoimmune pancreatitis.

Rheumatology key message

- Relapse predictors in IgG4-related disease without organ involvement at diagnosis were male sex and younger onset.

Funding: This work was supported by the Research on Measures for Intractable Diseases Project matching fund subsidy from the Ministry of Health, Labour, and Welfare, Japan.

Disclosure statement: The authors have declared no conflicts of interest.

References

1 Yamamoto M, Takahashi H, Shinomura Y. Mechanisms and assessment of IgG4-related disease: lessons for the rheumatologist. Nat Rev Rheumatol 2014;10:148–59.

2 Shimizu Y, Yamamoto M, Naishiro Y *et al.* Necessity of early intervention for IgG4-related disease—delayed treatment induces fibrosis progression. Rheumatology 2013;52:679–83.

3 Yamamoto M, Harada S, Ohara M *et al.* Beneficial effects of steroid therapy for Mikulicz's disease. Rheumatology 2005;44:1322–3.

4 Khosroshahi A, Stone JH. Treatment approaches to IgG4-related systemic disease. Curr Opin Rheumatol 2011;23:67–71.

5 Yamamoto M, Takahashi H, Ishigami K *et al.* Relapse patterns in IgG4-related disease. Ann Rheum Dis 2012;71:1755.

6 Gilmore W, Weiner LP, Correale J. Effect of estradiol on cytokine secretion by proteolipid protein-specific T cells clones isolated from multiple sclerosis patients and normal control subjects. J Immunol 1997;158:446–51.

7 Piccini MP, Giudizi MG, Biagiotti R *et al.* Progesterone favors the development of human T helper cells producing Th2-type cytokines and promotes both IL-4 production and membrane CD30 expression in established Th1 cell clones. J Immunol 1995;155:128–33.

8 Araneo BA, Dowell T, Diegel M, Daynes RA. Dihydrotestosterone exerts a depressive influence on the production of interleukin-4 (IL-4), IL-5, and gamma-interferon, but not IL-2 by activated murine T cells. Blood 1991;78: 688–99.

9 Tanaka A, Moriyama M, Nakashima H *et al*. Th2 and regulatory immune reactions contribute to IgG4 production and the initiation of Mikulicz's disease. Arthritis Rheum 2012;64:254–63.

10 Kamisawa T, Okazaki K, Kawa S *et al*. Japanese consensus guidelines for management of autoimmune pancreatitis: III. Treatment and prognosis of AIP. J Gastroenterol 2010;45: 471–7.

Japan College of Rheumatology
MODERN RHEUMATOLOGY

http://informahealthcare.com/mor
ISSN 1439-7595 (print), 1439-7609 (online)

Mod Rheumatol, 2015; Early Online: 1–2

DOI: 10.3109/14397595.2014.995893

informa
healthcare

LETTER

Seasonal allergies and serial changes of serum levels of IgG4 in cases treated with maintenance therapy for IgG4-related disease

Motohisa Yamamoto[1], Hiroki Takahashi[1], Yui Shimizu[1], Hidetaka Yajima[1], Chisako Suzuki[1], Yasuyoshi Naishiro[1], Kohzoh Imai[2], and Yasuhisa Shinomura[1]

[1]*Department of Gastroenterology, Rheumatology and Clinical Immunology, Sapporo Medical University School of Medicine, Sapporo, Hokkaido, Japan, and* [2]*The Institute of Medical Science, The University of Tokyo, Bunkyo, Tokyo, Japan*

Keywords
Allergen, Glucocorticoid, IgE, IgG4, IgG4-related disease

History
Received 18 November 2014
Accepted 3 December 2014
Published online 9 January 2015

To the Editor,

Immunoglobulin G4-related disease (IgG4-RD) is a chromic and inflammatory disease that results in irreversible organ dysfunction in the long term due to helper T type 2 (Th2) inflammation and fibrosis [1]. Glucocorticoid treatment is useful for the induction of remission, but the disease tends to relapse upon tapering off of steroid treatment [2]. There is no biomarker for disease activity of IgG4-RD at this time. Tabata et al. reported that the serial changes of serum IgG4 levels could predict the recurrence of IgG4-RD [3], but in daily practice we have often seen relapse without elevation of serum IgG4 levels, as well as mild elevation of serum IgG4 levels without relapse. Meanwhile, an association of IgG4-RD with allergy has been suggested [4]. To address these issues, we analyzed the relationships between serum IgG4 levels and seasonal allergens in IgG4-RD. This retrospective study was performed in compliance with applicable ethical regulations, as certified by our hospital's Institutional Review Board.

The subjects were the 62 IgG4-RD cases who met the comprehensive diagnostic criteria for IgG4-RD [5]. The cases were sorted according to presentation in 2013 using the following classifications: no relapse; steroid dose changed by 2 mg/day or less; and no prescription of rituximab. We checked specific allergens before treatments, and measured the levels of serum IgG4 and IgE at each visit. We analyzed whether the peak levels of these two Igs coincided with allergen release (i.e., pollen scattering) periods. The specific allergens tested were as follows: seasonal allergens of *Betula verrucosa* (Bet v 1), *Cryptomeria japonica* (Cry j 1/Cry j 2), *Tinea translucens* (Tin t 1), *Dactylis glomerata* (Dac g 1), *Phleum pratense* (Phl p1/Phl p 12), *Anthoxanthum odoratum* (Ant o 1), *Ambrosia artemisiifolia* (Amb a 1), *Artemisia vulgaris* (Art v 1), *Leucanthemum vulgare* (Leu v 1), and perennial allergens of *Dermatophagoides pteronyssinus* (Der p 1/Der p 2), *Canis familiaris* (Can f 1), *Felis domesticus* (Fel d 1), *Candida albicans* (Can a 1), *Aspergillus fumigatus* (Asp f 1), and *Penicillium citrinum* (Pen c 3). The levels of serum IgG4 were measured by nephelometry; levels of IgE were measured by fluorescence-enzyme immunoassay; and levels of allergen-specific IgE were measured by radio-immunosorbent test. Serial changes of IgG4 and IgE were defined as fluctuations of over 20% from the mean concentration across all visits. Specific IgE concentrations of >0.70 UA/mL were defined as positive reactions for the allergens.

Seven (11.3%) of the 62 cases exhibited positive response for seasonal allergens only. These positive responses consisted of four cases harboring IgE for *B. verrucosa* (Bet v 1), and three harboring IgE for *D. glomerata* (Dac g 1). In Northern Japan (the location of this study), *B. verrucosa* pollen is released in May, while *D. glomerata* pollen is released between June and July. They showed clinical symptoms, including rhinorrhea and rhinostenosis in these seasons, but they were not prescribed with both anti-allergy medication and glucocorticoid. The levels of serum IgG4 in all of these cases were elevated in the respective seasons (Figure 1). Two of them showed IgE for several seasonal allergens, but it was considered that there was less effect on this analysis because the titers of IgE for Bet v 1 were significantly higher than those of the other allergens. On the other hand, twenty-five (40.3%) of the 62 cases exhibited serial changes of IgG4 levels. The fluctuation ranges were larger in proportion to the levels of serum IgG4 at the time of diagnosis. There were, of course, no relapsed cases. 25 cases with allergies to perennial allergens or without allergies did not show these serial changes. With regard to IgE, most cases (with or without allergies) exhibited less changes in IgE levels or discrepancy between the peak of IgE levels and the allergens-scattering period.

This study revealed that serum IgG4 levels also correlated with seasonal allergies in subset of cases with IgG4-RD.

Correspondence to: Motohisa Yamamoto, Department of Gastroenterology, Rheumatology and Clinical Immunology, Sapporo Medical University School of Medicine. South 1- West 16, Chuo-ku, Sapporo, Hokkaido, 0608543, Japan. Tel: + 81-11-611-2111. Fax: + 81-11-611-2282. E-mail: mocha@cocoa.plala.or.jp

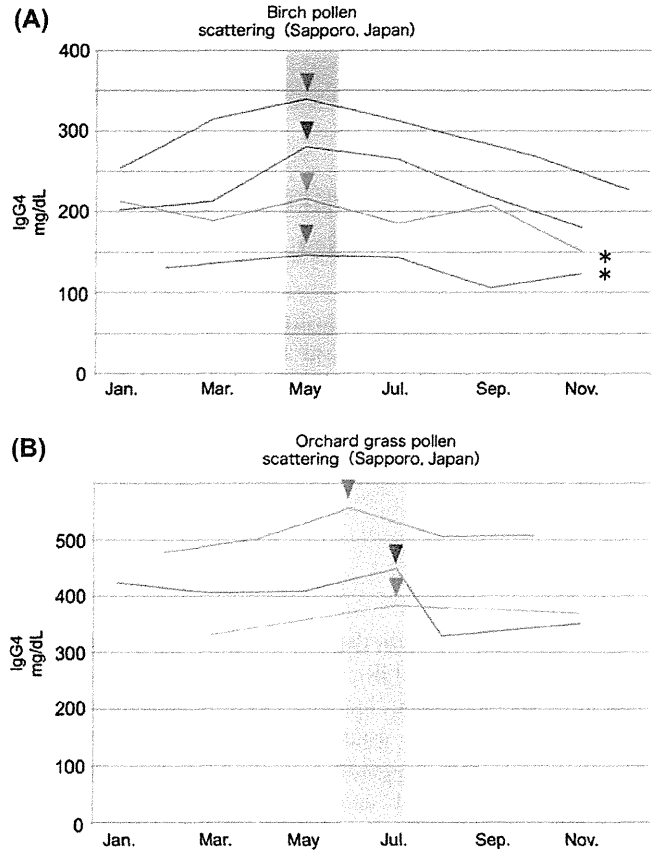

Figure 1. Seasonal changes of the levels of serum IgG4 in IgG4-related disease. (A) *B. verrucosa* pollen, (B) *D. glomerata* pollen. Serum IgG4 levels peaked during the pollen release periods of the seasonal allergens in the cases with the seasonal changes of serum IgG4 levels. The cases with asterisk had IgE for several seasonal allergens.

A quarter of the cases presented with allergies against both seasonal and perennial allergens; these cases therefore were excluded from this analysis. The final number of analyzable cases was small because of the exclusion of patients with low allergen titers, but we noted that the peak of serum IgG4 concentrations coincided with the scattering period of allergens in all cases that presented with serial changes in IgG4 levels and positive for IgEs against seasonal allergens. We hypothesize that seasonal allergies affected the production of IgG4 in these cases.

The physiology of IgG4 is still unknown, but this Ig has been proposed to be a blocking antibody for IgE [6]. We also measured serum IgE levels in the cases with seasonal allergies, but seasonal changes were not observed. The lack of seasonal changes likely reflects the vivo half-life time of IgE. The half-life of IgG4 is estimated as approximately 21 days, while that of IgE is only 2 days; thus levels of the latter are expected to decrease rapidly in the absence of exposure to allergens [7]. It is possible that peak IgE levels could not be accurately measured during the scattering periods of the allergens.

Terao et al. reported that serum IgG levels show seasonal changes in patients with autoimmune diseases [8]. It is unknown at this point whether the levels of serum IgG4 in healthy controls exhibit seasonal changes, but we found that serum IgG4 levels in some IgG4-RD cases with maintenance therapy or discontinuing steroid were transiently affected by the seasonal allergies. This phenomenon may complicate clinical evaluation, especially for cases where IgG4-RD disease activity is detected only by levels of serum IgG4. The clinical significance of the serial changes of serum IgG4 levels during treatment for IgG4-RD will require further investigation. Additional data will be needed to define useful biomarkers for IgG4-RD.

Funding

This work was supported by the Research on Measures for Intractable Diseases Project matching fund subsidy from Ministry of Health Labour and Welfare, Japan.

Conflict of interest

None.

References

1. Shimizu Y, Yamamoto M, Naishiro Y, Sudoh G, Ishigami K, Yajima H, et al. Necessity of early intervention for IgG4-related disease – delayed treatment induces fibrosis progression. Rheumatology (Oxford). 2013;52(4):679–83.
2. Yamamoto M, Takahashi H, Shinomura Y. Mechanisms and assessment of IgG4-related disease: lessons for the rheumatologist. Nat Rev Rheumatol. 2014;10(3):148–59.
3. Tabata T, Kamisawa T, Takuma K, Egawa N, Setoguchi K, Tsuruta K, et al. Serial changes of elevated serum IgG4 levels in IgG4-related systemic disease. Intern Med. 2011;50(2):69–75.
4. Masaki Y, Dong L, Kurose N, Kitagawa K, Morikawa Y, Yamamoto M, et al. Proposal for a new clinical entity, IgG4-positive multi-organ lymphoproliferative syndrome: Analysis of 64 cases of IgG4-related disorders. Ann Rheum Dis. 2009;68(8):1310–5.
5. Umehara H, Okazaki K, Masaki Y, Kawano M, Yamamoto M, Saeki T, et al. Comprehensive diagnostic criteria for IgG4-related disease (IgG4-RD), 2011. Mod Rheumatol. 2012;22(1):21–30.
6. Aalberse RC, Stapel SO, Schuurman J, Rispens T. Immunoglobulin G4: an odd antibody. Clin Exp Allergy. 2009;39(4):469–77.
7. Hamilton RG. Chapter 3. Human Immunoglobulin. In: Leffell MS, Donnenberg AD, Rose NR, editors. Handbook of Human Immunology, 1 ed. Boca Raton FL: CRC Press, 1997:65–110.
8. Terao C, Ohnuma K, Yamamoto K, Yukawa N, Kawabata D, et al. Serum IgG levels demonstrate seasonal change in connective tissue disease: a large-scale, 4-year analysis in Japanese. Mod Rheumatol. 2012;22(3):426–30.

J Gastroenterol
DOI 10.1007/s00535-015-1049-0

The Japanese Society of Gastroenterology

ORIGINAL ARTICLE—ALIMENTARY TRACT

Contextual niche signals towards colorectal tumor progression by mesenchymal stem cell in the mouse xenograft model

Suguru Nakagaki · Yoshiaki Arimura · Kanna Nagaishi · Hiroyuki Isshiki · Masanao Nasuno · Shuhei Watanabe · Masashi Idogawa · Kentaro Yamashita · Yasuyoshi Naishiro · Yasushi Adachi · Hiromu Suzuki · Mineko Fujimiya · Kohzoh Imai · Yasuhisa Shinomura

Received: 15 December 2014 / Accepted: 24 January 2015

Abstract
Background The role of mesenchymal stem/stromal cells (MSCs) in tumorigenesis remains controversial. This study aimed to determine whether heterotypic interactions between MSCs and colon cancer cells can supply contextual signals towards tumor progression.
Methods Xenografts consisting of co-implanted human colorectal cancer cells with rat MSCs in immunodeficient mice were evaluated by tumor progression, angiogenic profiles, and MSC fate. Furthermore, we investigated how MSCs function as a cancer cell niche by co-culture experiments in vitro.
Results Tumor growth progressed in two ways, either independent of or dependent on MSCs. Such cell line-specific dependency could not be explained by host immune competency. COLO 320 xenograft angiogenesis was MSC-dependent, but less dependent on vascular endothelial growth factor (VEGF), whereas HT-29 angiogenesis was not MSC-dependent, but was VEGF-dependent. MSCs and COLO 320 cells established a functional positive feedback loop that triggered formation of a cancer cell niche, leading to AKT activation. Subsequently, MSCs differentiated into pericytes that enhanced angiogenesis as a perivascular niche. In contrast, the MSC niche conferred an anti-proliferative property to HT-29 cells, through mesenchymal–epithelial transition resulting in p38 activation.
Conclusions In conclusion, MSCs demonstrate pleiotropic capabilities as a cancer cell or perivascular niche to modulate colorectal cancer cell fate in a cell line-dependent manner in a xenogeneic context.

Keywords Mesenchymal stem cell · Niche · Pericyte · Cancer-associated fibroblast · Angiogenesis

S. Nakagaki and Y. Arimura contributed equally to this work.

Electronic supplementary material The online version of this article (doi:10.1007/s00535-015-1049-0) contains supplementary material, which is available to authorized users.

S. Nakagaki · Y. Arimura (✉) · H. Isshiki · M. Nasuno · S. Watanabe · K. Yamashita · Y. Adachi · Y. Shinomura
Department of Gastroenterology, Rheumatology, and Clinical Immunology, Sapporo Medical University, Sapporo 060-8543, Japan
e-mail: arimura@sapmed.ac.jp

K. Nagaishi · M. Fujimiya
Department of Anatomy, Sapporo Medical University, Sapporo 060-8543, Japan

M. Idogawa
Department of Medical Genome Sciences, Research Institute for Frontier Medicine, Sapporo Medical University, Sapporo 060-8543, Japan

Y. Naishiro
Department of Educational Development, Sapporo Medical University, Sapporo 060-8543, Japan

H. Suzuki
Department of Molecular Biology, Sapporo Medical University, Sapporo 060-8543, Japan

K. Imai
Center for Antibody and Vaccine Therapy, The University of Tokyo, Tokyo 108-8639, Japan

Published online: 14 February 2015

Abbreviations

MSCs	Mesenchymal stem/stromal cells
TME	Tumor microenvironment
CAFs	Cancer-associated fibroblastic cells
CCL5	C–C motif chemokine ligand 5
EMT	Epithelial–mesenchymal transition
IL-6	Interleukin-6
VEGF	Vascular endothelial growth factor
eGFP	Enhanced green fluorescence protein
αMEM	α-Modified Eagle's medium
FBS	Fetal bovine serum
qRT-PCR	Quantitative real-time reverse transcription PCR
MVD	Tumor microvessel density
Thy-1	Thymus cell antigen-1
NG2	Neural/glial antigen 2
αSMA	α-Smooth muscle actin
OE	Overexpression
CXCL12	Chemokine C-X-C motif ligand 12
KD	Knock down
MSC-CM	MSC-conditioned medium
CXCR4	C-X-C chemokine receptor type 4
MAPKs	Mitogen-activated protein kinases
FACS	Fluorescence-activated cell sorting
ANOVA	Analysis of variance
PECAM-1	Platelet endothelial cell adhesion molecule-1
Vegfr1 (Flt1)	Vascular endothelial growth factor receptor 1
PDGF-BB	Platelet-derived growth factor BB
Pdgfr-β	Platelet-derived growth factor receptor-β
MET	Mesenchymal–epithelial transition
Vcam1	Vascular cell adhesion molecule-1
CCR5	Chemokine (C–C motif) receptor 5
VLA-4	Very late antigen-4

Introduction

Carcinogenesis, which is often accompanied by well-orchestrated desmoplastic reactions [1] involving the recruitment of bone marrow-derived mesenchymal stem/stromal cells (MSCs) [2], closely resembles wound healing and scar formation [3]. The stromal component of the tumor microenvironment (TME), which influences the malignant phenotype, consists of three general cell types: cancer-associated fibroblastic cells (CAFs), angiogenic vascular cells, and infiltrating immune cells [4]. However, the precise role of repopulating MSCs in tumorigenesis remains controversial. Khakoo et al. [5] demonstrated that MSCs possess intrinsic, anti-neoplastic properties by inhibiting AKT activity in an E-cadherin-mediated, cell–cell contact-dependent manner. They suggested that MSCs might be useful for treating human malignancies characterized by AKT dysregulation. In contrast, Karnoub et al. [6] demonstrated that the microenvironment of MSCs within the tumor stroma in SCID mice facilitated metastatic spread by paracrine signaling of C–C motif chemokine ligand 5 (CCL5) secreted de novo by MSCs.

Although MSCs are prime candidates for cell-based therapies [7, 8] of a variety of diseases, our understanding of the interactions between colorectal cancer cells and MSCs remain limited [9]. Recent studies have focused disproportionately on the protumorigenic role of MSCs in colorectal cancer growth by differentiation into CAFs, secretion of key paracrine factors, or induction of epithelial–mesenchymal transition (EMT) [10–16]. Tsai et al. [10] and Shinagawa et al. [11] reported that MSCs differentiate into CAFs in the tumor stroma. Similarly, De Boeck et al. [12] showed that MSCs are a source of tumor-associated mesenchymal cells that drive tumor progression. In contrast, Lin et al. [13] isolated MSC-like cells from colon cancer tissues and demonstrated the importance of interleukin-6 (IL-6)/Notch-1/CD44 signals in colon cancer progression. Liu et al. [14] reported that stimulated MSCs in the TME express higher levels of vascular endothelial growth factor (VEGF), which enhances tumor angiogenesis. Furthermore, Li et al. [15] emphasized that such protumorigenic effects of MSCs induced activation of β-catenin signaling. Finally, Mele et al. [16] reported that MSCs induce EMT in human colorectal cancer cells.

Therefore, our goal was to determine whether MSCs could supply contextual signals that promote or suppress colorectal tumor progression. To this end, we hypothesized that MSCs could create a cancer cell niche to modulate colorectal cancer growth in a context-dependent manner. Consequently, we found that MSCs could have multiple effects on colon cancer progression in the xenograft model. Such knowledge of the multifaceted roles of MSCs in colorectal cancer is important before exploring the broader clinical applications of MSC-based therapies.

Methods

For detailed Methods, please refer to the Supplementary Material.

Experimental animals

Lewis rats were purchased from Charles River Laboratories Japan (Yokohama, Japan). SD-TG [CAG-enhanced green fluorescence protein (eGFP)] rats [17] and athymic nude (BALB/cSlc-nu/nu) mice were obtained from Japan SLC

Inc. (Hamamatsu, Japan). NOG mice (NOD/Shi-scid, IL-2Rγnull) [18] were purchased from the Central Institute of Experimental Animals (Kawasaki, Japan). FOX CHASE SCID C.B-17/Icr-scid/scidJcl mice were from CLEA Japan Inc. (Tokyo, Japan). All animal studies were performed under the supervision of the Committee for Animal Research Center of Sapporo Medical University and in accordance with protocols approved by the Institutional Animal Care and Use Committee. The animals were maintained according to the guidelines of the University Committee for Animal Research.

Cell lines and culture conditions

The six human colorectal cancer cell lines used in the xenograft experiments were purchased from the American Type Culture Collection (ATCC; Manassas, VA, USA), RIKEN BioResource Center (Tsukuba, Japan), or the Japanese Collection of Research Bioresources (Osaka, Japan). All cell lines, LoVo (DSMZ ACC 350), HCT116 (ATCC: CCL 247), COLO 320 (DSMZ ACC 144), DLD-1 (ATCC: CCL 221), HCT-15 (ATCC: CCL 225), and HT-29 (DSMZ ACC 299), were cultured under conditions recommended by their supplier.

Isolation and culture of rat MSCs

Briefly, bone marrow cells were harvested by inserting a needle into the shafts of femurs and tibiae, and flushing with 30 mL complete α-modified Eagle's medium (αMEM) containing 20 % fetal bovine serum (FBS). Cell suspensions were filtered through a 70-μm nylon filter (Becton–Dickinson, Franklin Lakes, NJ, USA) and seeded in 75 cm^2 flasks. The cells were grown in complete αMEM containing 20 % FBS at 37 °C in a humidified atmosphere with 5 % CO_2. After 3 days, the medium was replaced with fresh medium containing 10 % FBS, and the adherent cells were grown to 80 % confluence for passage 0. In accordance with the criteria of the International Society for Cellular Therapy [19], cells at passage 3–5 were used in subsequent experiments. eGFP-labeled MSCs were harvested from CAG-eGFP rats and cultured as described above [20]. Immunophenotyping and in vitro differentiation capacity of MSCs were determined as described in Supplementary Material.

Xenograft model and evaluation of tumor growth

For xenograft experiments, viable colon cancer cells were inoculated alone or together with rat GFP-labeled MSCs by subcutaneous injection into recipient NOG, SCID, and nude mice. Animals were observed daily, and tumor volumes were measured in two dimensions three times weekly using precision calipers. The tumor volume was calculated and expressed as the mean ± SEM from five mice in each group as described previously [21]. The two most distinctive cell lines underwent subsequent xenograft analyses using nude, SCID, and NOG mice, namely, COLO 320 as an MSC-dependent cell line and HT-29 as an MSC-independent cell line as described above. The ratio of MSCs to colon cancer cells was 1:1, unless otherwise indicated, as described elsewhere in detail (Supplementary Fig. 1a, b).

RNA isolation and quantitative real-time reverse transcription PCR (qRT-PCR) analysis

Total RNA was extracted using an RNeasy Mini Kit (Qiagen, Hilden, Germany), and 500 ng of total RNA was reverse transcribed into cDNA with oligo-dT primers using SuperScriptIII Reverse Transcriptase (Invitrogen, Carlsbad, CA, USA). The primers are described in Supplementary Table 1. Human *GAPDH* and rat *Gapdh* primers were used as an internal standard for the integrity and quantity of RNA. Quantitative real-time reverse transcription PCR (qRT-PCR) was performed using a GeneAmp 7000 Sequence Detection System (Applied Biosystems) with TaqMan Universal PCR Master Mix (Applied Biosystems) for 40 cycles of a two-step PCR amplification protocol (95 °C for 15 s and 60 °C for 1 min). Data were analyzed using the $^{\Delta\Delta}C_t$ method [22]. qRT-PCR was performed in triplicate unless otherwise indicated.

Evaluation of tumor microvessel density

Tumor microvessel density (MVD) (microvessel/mm^2) of the entire tumor area was evaluated using a previously described method [23]. Two independent observers counted the number of microvessels in the entire field of the tumor. MVD of specimens was calculated as the mean MVD of triplicates.

Characterization of eGFP-labeled rat MSC-derived cells in xenografts

eGFP fluorescence and primary antibodies against thymus cell antigen-1 (Thy-1, CD90), neural/glial antigen 2 (NG2) chondroitin sulfate proteoglycan, CD31, von Willebrand factor, α-smooth muscle actin (αSMA), desmin, vimentin, and RM-4 [24] (Supplementary Table 2) were used for immunofluorescence analyses together with Alexa Fluor 594-labeled secondary antibodies.

Two-color fluorescence in situ hybridization (FISH) analysis

Two-color FISH of human colorectal cancer xenografts subcutaneously implanted into SCID mice with or without

rat MSCs has been described previously [25]. Nuclei were counterstained with DAPI. Positive fluorescence signals appeared as multiple dots in the nucleus. Green and yellow indicated rat and mouse chromosomes, respectively. For simultaneous analysis of immunofluorescence and FISH on the same sections, immunofluorescence was performed prior to FISH to avoid attenuation of antigenicity.

Chemotaxis assays

We used recombinant human chemokine (C-X-C motif) ligand 12 (CXCL12)/stromal derived factor-1α [SDF-1α (PeproTech Inc., Rocky Hill, NJ, USA)], VEGF (Abnova, Taipei, Taiwan), platelet-derived growth factor BB (PDGF-BB), or IL-6 (PeproTech) as chemoattractants. For MSC migration assays, 3×10^5 eGFP-labeled MSCs were seeded in the upper well of a 24-well Transwell Boyden chamber (polycarbonate membranes, 8.0-μm pore size; Corning, Lowell, MA, USA) and allowed to migrate toward the bottom well containing serum-free medium with 100 ng/mL of the indicated chemoattractants for 24 h. Migrating cells were counted under a BZ-9000 BIOREVO all-in-one fluorescence microscope (Keyence, Osaka, Japan).

Microarray analysis

RNA was extracted from xenografts of COLO 320 cells alone or COLO 320 cells co-implanted with rat MSCs from NOG mice using an RNeasy kit and analyzed with a Human Oligo chip 25 K 3D-Gene (Toray, Tokyo, Japan).

Transcript Profiling: Accession No: GSE29389.

Cell transduction

To generate stable VEGF over-expressing (VEGF OE) and CXCL12 knockdown (CXCL12 KD) cell lines, COLO 320 cells were transduced with lentiviruses for VEGF or CXCL12 shRNA expression (GenTarget, San Diego, CA, USA) for 72 h according to the manufacturer's instructions. These stable cell lines were subjected to the xenograft analysis in SCID mice as described previously. The total number of mice used in this experiment was 15.

Co-culture of human colon cancer cell lines with rat MSCs

To examine heterotypic interactions between colon cancer cells and MSCs, MSCs were co-cultured with COLO 320 and HT-29 colon cancer cells either directly or indirectly using a Transwell culture dish. Moreover, monocultured colon cancer cells were treated with MSC-conditioned medium (MSC-CM) or recombinant human CXCL12. Co-cultured COLO 320 cells were also treated with neutralizing antibodies against human E-cadherin (Takara, Otsu, Japan), CCL5 (R&D Systems Inc., Minneapolis, MN, USA), or CD49d (α4 integrin, Pierce Biotechnology, Rockford, IL, USA) (Supplementary Table 2), or a small molecule antagonist of CXCR4, AMD3100 (Sigma-Aldrich, Saint Louis, MO, USA), or an γ-secretase inhibitor [(3,5-difluorophenylacetyl)-Ala-Phg-OBu, DAPT, PEPTIDE, Minoh, Japan].

Cell cycle analysis and apoptosis

Cell cycle distribution was analyzed by flow cytometry and Ki-67 immunohistochemistry (Abcam, Cambridge, MA, USA) (Supplementary Table 2). Ki-67 immunohistochemistry was performed according to the manufacturer's instructions. Apoptosis was measured by terminal deoxynucleotidyl transferase-mediated dUTP nick-end labeling (TUNEL) reactions using the DeadEnd Colorimetric TUNEL system (Promega, Madison, WI, USA).

Western blot analysis of AKT, mitogen-activated protein kinases (MAPKs), and EMT signaling molecules

Each cell population separated by FACS was lysed in radioimmunoprecipitation assay buffer comprising 20 mM Tris–HCl (pH 7.4), 150 mM sodium chloride, 1 mM EDTA (pH 8.0), 0.1 % (w/v) SDS, 0.1 % sodium deoxycholate, 1 % Triton X-100, and one tablet each of complete Mini protease inhibitor cocktail and PhosSTOP phosphatase inhibitor cocktail tablets (Roche Diagnostics, Mannheim, Germany). Forty micrograms of each lysate, as determined by a Bio-Rad protein assay (Bio-Rad, Hercules, CA, USA), were resolved on a 12 % denaturing polyacrylamide gel and transferred to a polyvinylidene difluoride membrane. After blocking with 5 % nonfat dry milk in TBS, the membrane was incubated with primary antibodies against pan-AKT phospho-AKT (Ser473), JNK1/3, phospho-SAPK/JNK, p38, phospho-p38, SNAIL, E-cadherin, vimentin, or β-actin (Supplementary Table 2), followed by a horseradish peroxidase-conjugated secondary antibody (Santa Cruz Biotechnology, Santa Cruz, CA, USA). Immunoreactions were developed using an enhanced chemiluminescence kit (Amersham Biosciences, Little Chalfont, England).

Cell proliferation assay

COLO 320 cell proliferation was directly measured by flow cytometry. Briefly, co-cultured MSCs with or without neutralizing antibodies against human E-cadherin, CCL5, CD49d (α4 integrin), or γ-secretase inhibitor (DAPT), and

a small-molecule antagonist of CXCR4, AMD3100 were eliminated by gating GFP, and the viable single COLO 320 cell number was counted at 24, 48, and 72 h co-cultivation. These data were compared with the control of co-cultured COLO 320 without any treatments (Fig. 5c).

Statistical analysis

To compare two groups, parametric and nonparametric analyses were performed using the unpaired Student's *t* test and the Mann–Whitney *U* test, respectively. Categorical variables were compared using the Chi square test, the exact *P* value based on Pearson's statistic, or the Monte Carlo method. For multiple comparisons in in vivo studies, we employed analysis of variance (ANOVA), particularly in serial assessments, and two-way repeated measurements (mixed between or within subjects) ANOVA followed by Bonferroni's test. A difference was considered significant when P was < 0.05 in all two-tailed tests. Measured values obtained from the study are presented as mean ± standard error of means unless otherwise indicated. SPSS Statistics 17.0 software (SPSS Inc., Chicago, IL, USA) was used for all statistical analyses.

Results

MSC dependency for xenograft tumor progression

Xenografted tumor growth appeared to occur as two categories according to their dependency or lack of dependency on co-implanted MSCs. DLD-1, HCT-15, and HT-29 cells were MSC-independent, whereas COLO 320, HCT116, and LoVo cells were MSC-dependent in SCID mice (horizontal panels in Fig. 1a). We chose the two most distinctive cell lines, COLO 320 as an MSC-dependent cell line and HT-29 as an MSC-independent cell line, for subsequent analyses. To differentiate the effects of tumor immune surveillance from the net effects of MSCs on tumor progression, we examined three classes of immunodeficient mice as recipients of xenografts, namely nude mice, which have impaired T cell functions, SCID mice with impaired T cell and B cell functions, and NOG mice. Compared with the NOD strain, NOG mice have decreased NK and macrophage activities, and are defective for T and B cell functions from the scid mutation and exhibit dendritic cell dysfunction from an IL-2Rγ mutation [18]. NOG mice show very limited transplantation rejection. Therefore, they are an excellent model for human xenograft studies. In nude mice (bottom panels in Fig. 1a), engraftment of xenografts was delayed for both MSC-dependent and -independent cell lines, resulting in a smaller maximum tumor volume than that in SCID and NOG mice on day 13. Furthermore, COLO 320 xenografts without MSCs were successfully engrafted into NOG mice at approximately 2 weeks after implantation (top right panel in Fig. 1a).

Angiogenic profiles of xenograft tumors

Measurement of angiogenesis is complicated by the fact that it is a dynamic process, although most studies to date have focused on the products of angiogenesis such as VEGF family proteins [26] and MVD, which are common endpoints for assessment of tumor vascularity [23]. Therefore, we evaluated the angiogenic profiles by the expression of VEGF and other angiogenic proteins, including HGF and FGF-2, as well as MVD. VEGF mRNA expression was significantly higher in HT-29 xenografts than in COLO 320 xenografts, while there was no difference between either xenograft with and without MSCs (Fig. 1b). VEGF protein expression was significantly higher in HT-29 cells (3.35 ± 0.15 ng/mL) than that in COLO 320 cells (1.26 ± 0.47 ng/mL, $P = 1.65E{-}4$), while HGF and FGF-2 proteins were produced at the same level in the two cell lines (Supplementary Fig. 1c, d). Although cancer cell nests were sparser, the surrounding tumor stroma with tumor microvessels was more abundant in COLO 320 + MSC xenografts than in HT-29 + MSC xenografts (Fig. 1c). 'Modified MVD' was significantly greater in COLO 320 xenografts (1.60 ± 0.07 mm^{-2}) than in HT-29 xenografts (0.87 ± 0.03 mm^{-2}, $P = 0.0026$; Fig. 1d). The number of MSC-derived (eGFP-positive) cells progressively increased as COLO 320 xenografts advanced, particularly at 15 mm in diameter, while the number of these cells was low in HT-29 xenografts regardless of tumor size (Fig. 1e). Although MSCs successfully engrafted, rat *Vegf* was not detected by qRT-PCR, suggesting that rat Vegf produced by engrafted MSCs was less likely to directly compensate for human VEGF in co-implanted COLO 320 xenografts (Fig. 1f). Consequently, these results suggest that angiogenesis in COLO 320 xenografts occurs less depending on VEGF than HT-29 xenografts.

Fate of co-implanted eGFP-labeled rat MSCs in xenograft tumors

Engrafted MSCs were randomly distributed in the COLO 320 xenograft tumor stroma, potentially as CAFs, as previously reported (data not shown). Excluding CAFs, MSC-derived cells were primarily located in perivascular regions on day 14 after implantation (Fig. 2a). Several differentiation markers for pericytes, including Thy-1 (CD90; Fig. 2b), NG2 (Fig. 2c), and αSMA (Fig. 2d), largely or partially co-localized with eGFP, while platelet endothelial

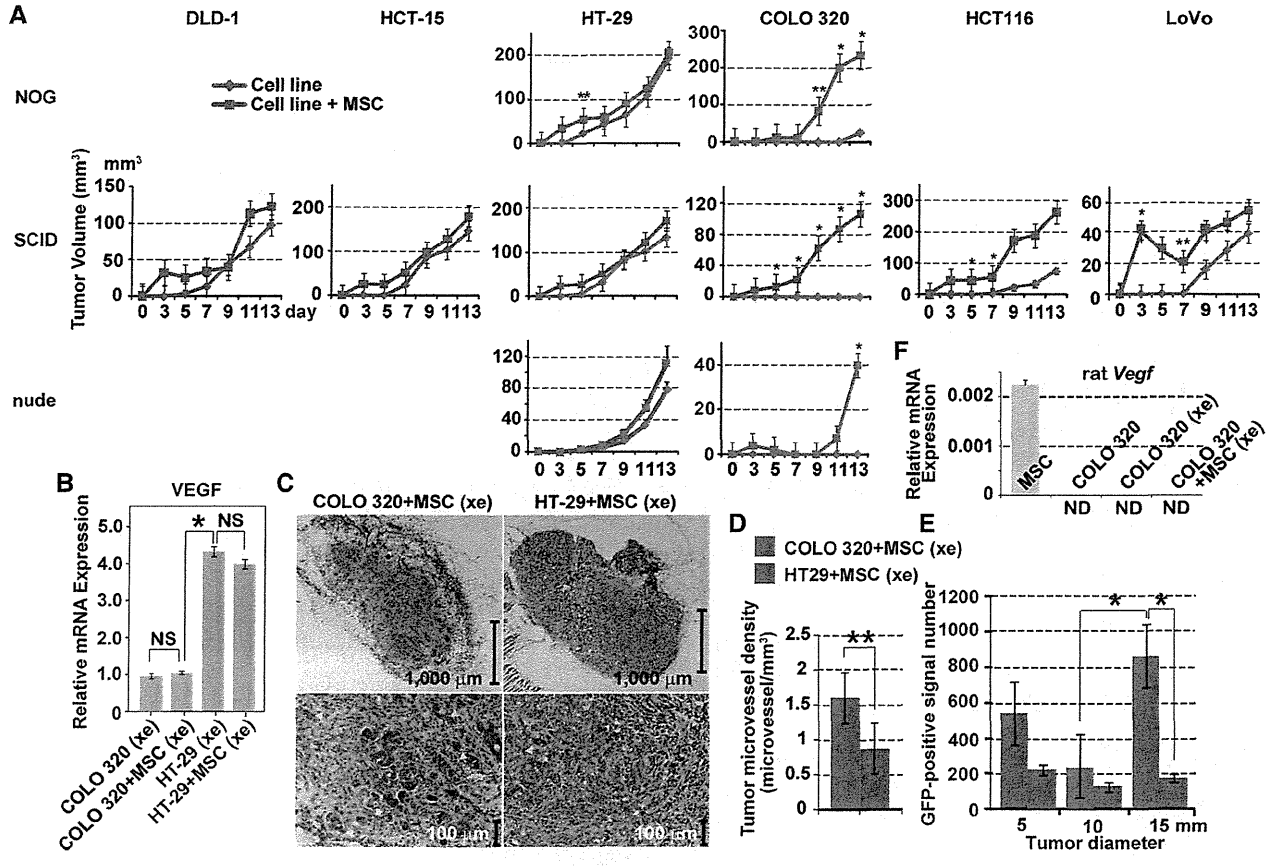

Fig. 1 Growth dependency and angiogenic profiles of MSC-co-implanted xenografts. **a** The tumor volume of xenografts established using six human colorectal cancer lines with or without co-implanted rat MSCs in the three class of immunodeficient mice was measured over 2 weeks. *Horizontal panels* designated as SCID show the dependency of tumor growth on co-implanted MSCs in all the six cell lines. MSC-independent cell lines were DLD-1, HCT-15, and HT-29 in SCID mice (*left half*), whereas MSC-dependent cell lines were COLO-320, HCT-116, and LoVo (*right half*). *Two rows of vertical panels* indicate HT-29 (*left*) and COLO-320 (*right*) xenograft analyses in the three class of immunodeficient mice. **b** VEGF transcripts were analyzed by qRT-PCR in xenografted tumors. **c** H&E-stained COLO-320 and HT-29 xenografts with co-implanted MSCs at low magnification (*upper panels*) and high magnification (*lower panels*). *Yellow arrowheads in the lower panels* indicate tumor vessels. **d** The modified MVD was estimated as the mean MVD of triplicates from COLO-320 and HT-29 cells. **e** Comparison of the number of GFP-positive signals obtained from tumors grown up to 5, 10, or 15 mm in diameter. The number of GFP-positive signals are expressed as mean ± SEM in three representative sections, respectively. **f** Relative rat-specific *Vegf* mRNA expression was compared in MSCs, COLO-320 cells, and COLO-320 xenografts with/without MSCs. *NS* and *ND* indicate 'not significant' and 'not detectable', respectively. *Asterisks* indicate statistical significance: $*P \leq 0.05$, $**P \leq 0.01$, $***P \leq 0.001$. **a** $P = 0.0048$ on day 5 of HT-29 xenografts in NOG mice; $P = 0.003$, 0.047, and 0.014 on days 9, 11, and 13 of COLO 320 xenografts in NOG mice; $P = 0.020$, 0.021, 0.013, 0.039, and 0.022 on days 5, 7, 9, 11, and 13 of COLO 320 xenografts in SCID mice; $P = 0.036$ on day 13 of COLO 320 xenografts in nude mice; $P = 0.017$ on day 5 and $P = 0.03$ on day 7 in the HCT-116 panel; $P = 0.025$ on day 3 and $P = 0.004$ on day 7 in the LoVo panel. **b** $P = 0.0048$ on day 5 of HT-29 xenografts in NOG mice. **e** $P = 0.043$ between 10 and 15 mm in the COLO 320 xenograft and $P = 0.031$ between COLO 320 and Ht-29 xenograft in 15 mm tumor diameter

cell adhesion molecule-1 (PECAM-1, CD31), a representative endothelial marker, did not co-localize, but was in close contact with eGFP-positive cells at the perivascular niche (Fig. 2e, f). These observations suggest that MSCs repopulate at the perivascular niche and differentiate into pericytes in COLO 320 xenograft tumors.

In contrast to COLO 320 xenografts, most MSCs were likely to engraft randomly as CAFs in the HT-29 xenograft tumor stroma (Fig. 2g), which partially expressed the representative myofibroblast marker, αSMA (Fig. 2h–k). Perivascular MSCs were seldom observed in HT-29 xenografts (Fig. 2l), while they were abundantly observed in COLO 320 xenografts.

Characterization of recruited mouse cells adjacent to rat MSC-derived cells

Rat MSCs were in line with or immediately adjacent to mouse cells (Fig. 3a, b). In simultaneous immunofluorescence analyses, mouse-derived cells recruited to the tumor

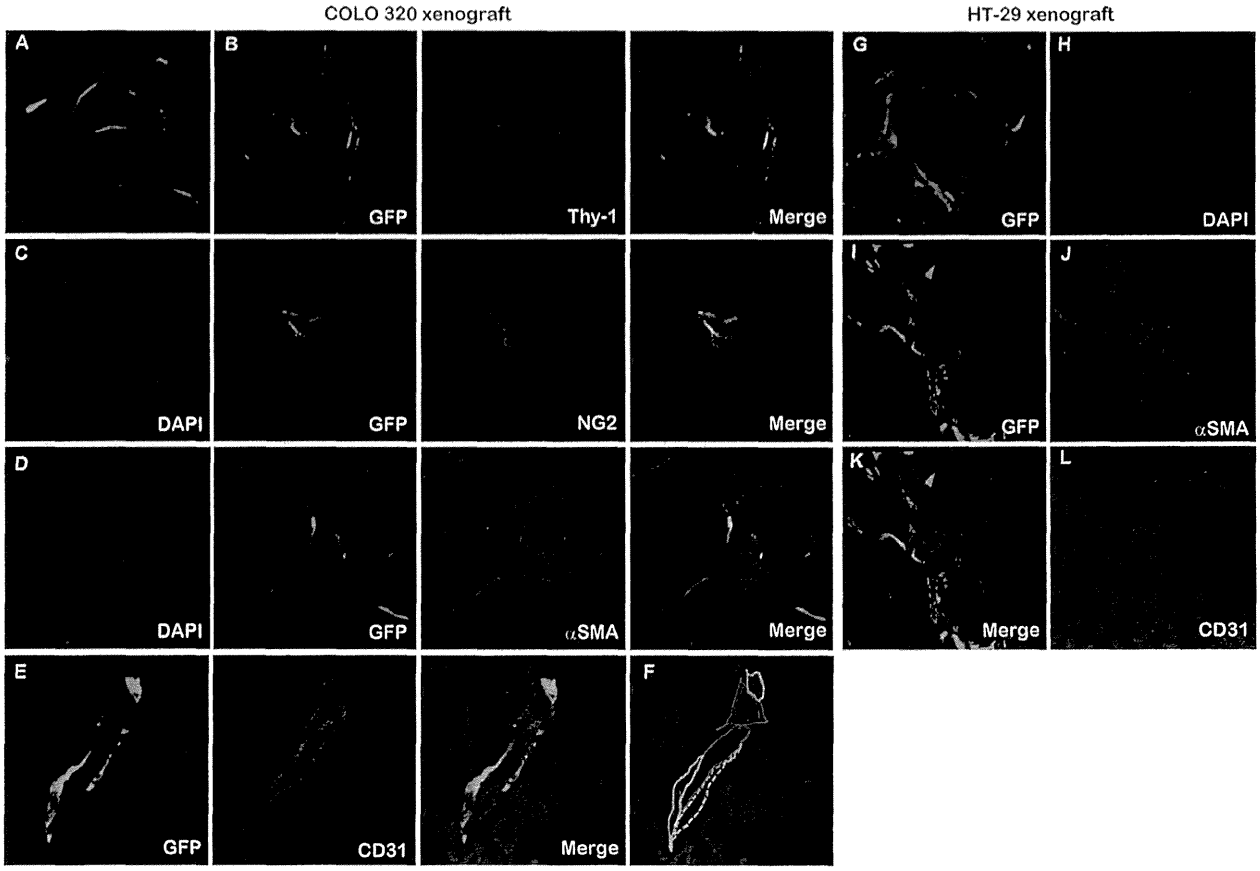

Fig. 2 Fate of GFP-positive MSC-derived cells in COLO-320 and HT-29 xenografts. **a** MSC-derived cells producing GFP fluorescence-populated areas along the inner vascular lumen in the COLO 320 tumor stroma. Cells were counterstained with DAPI. Pericyte markers, including Thy-1 (CD90) (**b**), NG2 chondroitin sulfate proteoglycan (**c**), and αSMA (**d**) were stained with Alexa Fluor 594-labeled antibodies in the COLO 320 tumor stroma. **f** Is a schematic representation of **e**. **g** MSC-derived cells producing GFP fluorescence randomly populated the HT-29 tumor stroma. **h** Cells were counterstained with DAPI. **j** αSMA was stained with an Alexa Fluor 594-labeled antibody. **k** Merged image of **h**–**j**. **l** Representative immunofluorescence of CD31 in the HT-29 tumor stroma

vessels differentiated mainly into CD31-positive endothelial cells (Fig. 3c), while some differentiated into αSMA-positive mural cells (Fig. 3d). These findings were more frequently observed in COLO 320 + MSC xenografts than in HT-29 + MSC xenografts (data not shown), which may explain why MVD was significantly greater in COLO 320 xenografts than in HT-29 xenografts, suggesting that rat MSC-derived cells recruited mouse angiogenic cells at possible sites of tumor vasculogenesis in COLO 320 xenografts. Whether these mouse cells are truly angiogenic cells or recruited at the site of tumor vasculogenesis should be warrant by further analysis.

Selective activation of the CXCL12/CXCR4 axis in COLO 320 xenografts co-implanted with MSCs

To investigate chemoattractants of rat MSCs, we evaluated ligand–receptor interactions for CXCL12/Cxcr4 [27], VEGF/Vegfr1(Flt1), Vegfr2 (Kdr) [26] PDGF-BB/Pdgfr-β [28], and IL-6/Il-6r α chain [29], all of which have been previously reported to act as MSC chemoattractants (Fig. 4a, b). Among these factors, human CXCL12 was unique and the most potent chemotactic factor to Cxcr4-bearing rat MSCs (Fig. 4c–f). qRT-PCR analysis revealed that *CXCL12* was the most upregulated gene among 58 upregulated genes of the 25,000 genes examined by microarray comparing co-implanted COLO 320 xenografts with COLO 320 xenografts alone (Fig. 4g, h). CXCL12 was expressed at baseline in COLO 320 cells and was not influenced by co-culture with MSCs; however, it was slightly upregulated in xenografts and dramatically upregulated in co-implanted xenografts, consistent with the transcriptomic data obtained from the microarray analysis. In contrast, HT-29 cells failed to express *CXCL12* under any of the conditions. *CXCR4* was slightly upregulated in co-cultured COLO 320 cells and markedly upregulated in

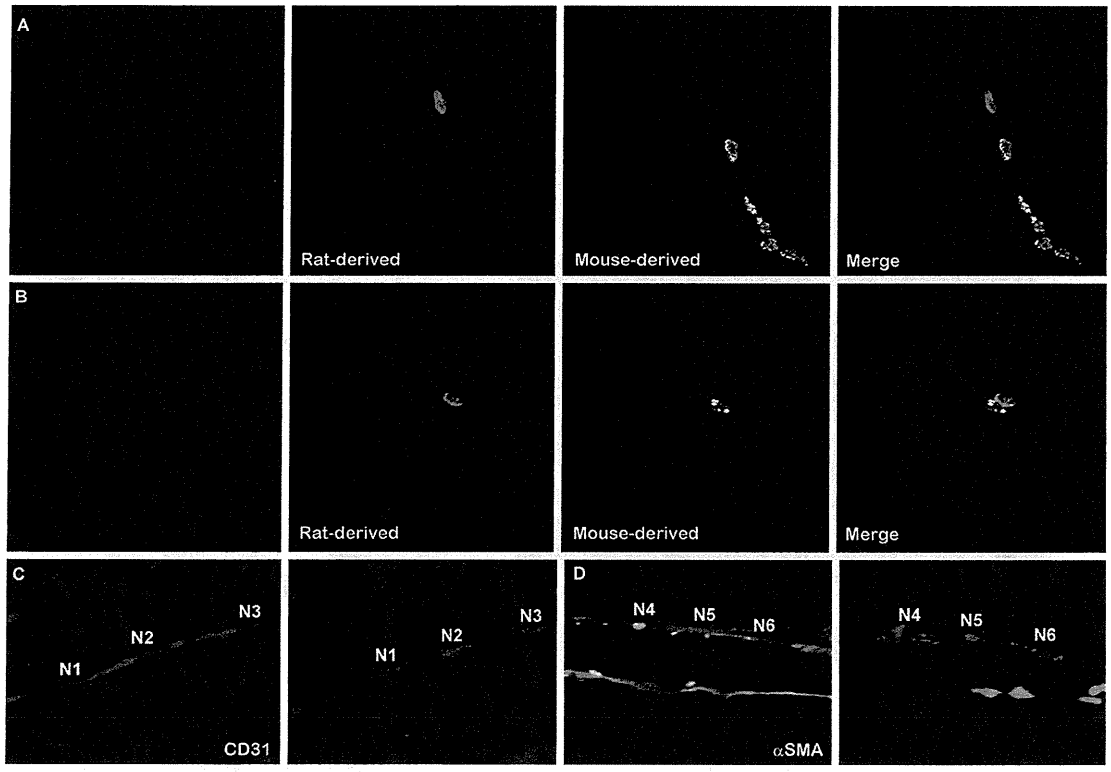

Fig. 3 Characterization of recruited mouse cells located adjacent to rat MSC-derived cells in COLO-320 xenografts. Using species-specific probes, we easily differentiated human, rat, and mouse cells in xenograft tumors by two-color FISH analysis (**a**, **b**) and simultaneous immunofluorescence analyses of CD31 (**c**) and αSMA (**d**) on the same sections analyzed by FISH. N1–6 in **c** and **d** indicate corresponding nuclei. MSC-derived cells produced green fluorescence from SpectrumGreen-labeled DNA probes while mouse angiogenic cells exhibited yellow fluorescence from Cy3-labeled DNA probes. Nuclei were counterstained with DAPI. *Pink signals in nuclei* indicate positive signals in FISH using the mouse-specific probe, while *red signals* in the cytoplasm indicate positive signals for CD31 (**c**) and αSMA (**d**) using immunofluorescence

xenografts with or without MSCs, whereas *CXCR4* was expressed at a low level in HT-29 cells under all conditions (Fig. 4i). Although analogous to rat *Vegf* (Fig. 1f), rat Cxcl12 produced by engrafted MSCs was less likely to directly compensate for tumor CXCL12 (Fig. 4j). However, in contrast to *Vegf*, rat MSCs significantly induced human *CXCL12* expression in xenograft tumors (Fig. 4i, $P = 0.017$).

To explore what attributes MSC-dependency to COLO 320 cells, we established CXCL12 knockdown (CXCL12 KD) and VEGF-overexpressing (VEGF OE) COLO 320 cells and initiated xenograft tumors using these stable lines. Xenograft tumor growth from the CXCL12 KD line was significantly inhibited; in contrast, tumor growth from the VEGF OE line was enhanced compared to that from mock transfectant. Either transgenic or knockdown cells as well as parental COLO 320 cells could not develop xenograft tumors without MSC co-implantation (Fig. 4k). These results suggested that tumor CXCL12 attributed MSC-dependent tumor growth to COLO 320 whereas tumor VEGF could not contribute to MSC-independent growth.

Interactions between rat MSCs and human colon cancer cell lines

Co-cultured MSCs significantly increased the Ki-67 labeling index of COLO 320 cells both at 48 h ($P = 0.044$) and 72 h ($P = 0.004$), while there was an increased apoptotic index of HT-29 cells at both 48 h ($P = 0.002$) and 72 h ($P = 0.006$, Fig. 5a). These data supported by cell cycle analysis (Supplementary Fig. 1d, e) suggest that MSCs as the cancer niche affected the proliferation of these tumor cell lines in quite different ways, with a protumorigenic effect on COLO 320 cells but an anti-tumorigenic effect on HT-29 cells. In COLO 320 cells, AKT protein was exclusively activated, or phosphorylated (Fig. 5b). This effect did not occur with indirect co-culture, MSC-CM, or recombinant CXCL12 treatment, but instead AKT was activated in the direct co-culture via a cell–cell contact-dependent mechanism with MSCs, namely, via a cancer niche. In sharp contrast to COLO 320 cells, MSCs suppressed AKT signaling but clearly activated or phosphorylated p38 in the co-cultured HT-29 cells in the cancer

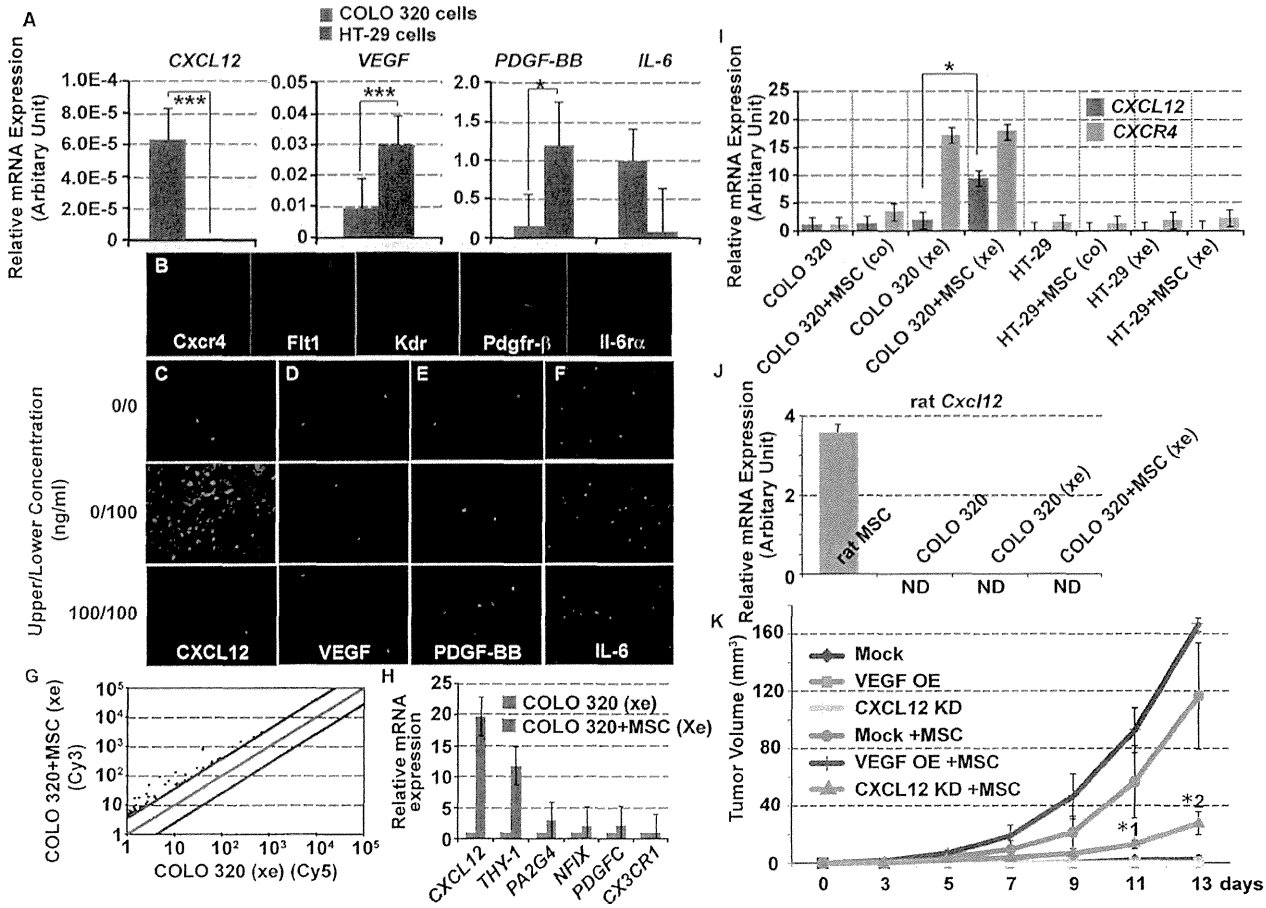

Fig. 4 Selective activation of the CXCL12/CXCR4 axis. **a** Ligand expression was analyzed by qRT-PCR in HT-29 and COLO-320 cells. CXCL12 and IL-6 transcripts were more abundant in COLO 320 cells, whereas VEGF and PDGF-BB transcripts were significantly more abundant in HT-29 cells. **b** Expression of receptors in rat MSCs was analyzed by immunofluorescence using Alexia Fluor 594-labeled secondary antibodies. All of the corresponding receptor proteins were expressed in rat MSCs at various levels. **c–f** Chemotaxis assays were conducted with GFP-labeled MSCs seeded in upper wells and allowed to migrate toward the bottom wells containing cell-free medium with 0–100 ng/mL recombinant human chemoattractants. The assay was performed in triplicate. **g** RNA extracted from xenografts of COLO-320 cells alone or co-implanted with rat MSCs in NOG mice was analyzed using a human Oligo chip 25 K 3D-Gene (Toray) microarray. By setting the cut-off value as greater than fourfold that of the expression difference in the microarray analysis, 58 of the 25,000 genes examined were found to be more upregulated in xenografts of COLO 320 cells co-implanted with rat MSCs than in COLO 320 xenografts alone. **h** The indicated six genes among all upregulated genes were confirmed by qPCR. **i** qRT-PCR analysis of the human CXCL12/CXCR4 axis under various conditions. **j** Rat-specific Cxcl12 mRNA expression was compared in rat MSCs, COLO-320 cells, and COLO-320 xenografts with/without MSCs. **k** Growth dependency of COLO 320 cells, in which VEGF was overexpressed or CXCL12 was knocked down, on rat MSCs. Mock represented cells transduced by negative control shRNA lentivector plasmid DNA. *ND* indicates 'not detectable' and *co* and *xe* represent 'co-culture with rat MSCs' and 'xenograft tumors,' respectively. *Asterisks* indicate statistical significance. **a** $P = 6.34E{-}4$ for CXCL12, $P = 5.53E{-}5$ for VEGF, $P = 0.018$ for PDGF, **i** $P = 0.017$, and **k** *1, VEGF OE vs. CXCL12 KD $P = 0.037$, CXCL12KD vs. VEGF OE + MSC $P = 0.037$; *2, Mock vs. CXCL12 KD $P = 0.039$, VEGF OE vs. CXCL12 KD $P = 0.002$, VEGF OE vs. CXCL12 KD + MSC $P = 0.011$, CXCL12 KD vs. Mock + MSC $P = 0.039$, CXCL12 KD vs. VEGF OE + MSC $P = 0.002$, VEGF OE + MSC vs. CXCL12KD + MSC $P = 0.011$. **k** Growth dependency of COLO 320 cells, in which VEGF was overexpressed or CXCL12 was knocked down, on rat MSCs. *OE* overexpression, *KD* knock down

niche (Fig. 5b). The cytokine-producing capacity of co-cultured MSCs was analyzed by qRT-PCR (Supplementary Fig. 1f). To confirm whether CXCL12 (Fig. 4i) or Cxcl12 (Supplementary Fig. 2a) worked as a component of the cancer niche, treatment of recombinant CXCL12 (Fig. 5b) and CXCR4 antagonist (AMD3100, Fig. 5c) was included in the analyses.

Relevant cancer cell niche signaling by MSCs

First, we chose relevant niche signaling molecules for the subsequent analyses from the candidate panel when ligands and/or receptors were upregulated in MSCs under co-cultivation with COLO 320 (Supplementary Fig. 2a). COLO 320 cell proliferation under direct contact with MSCs was

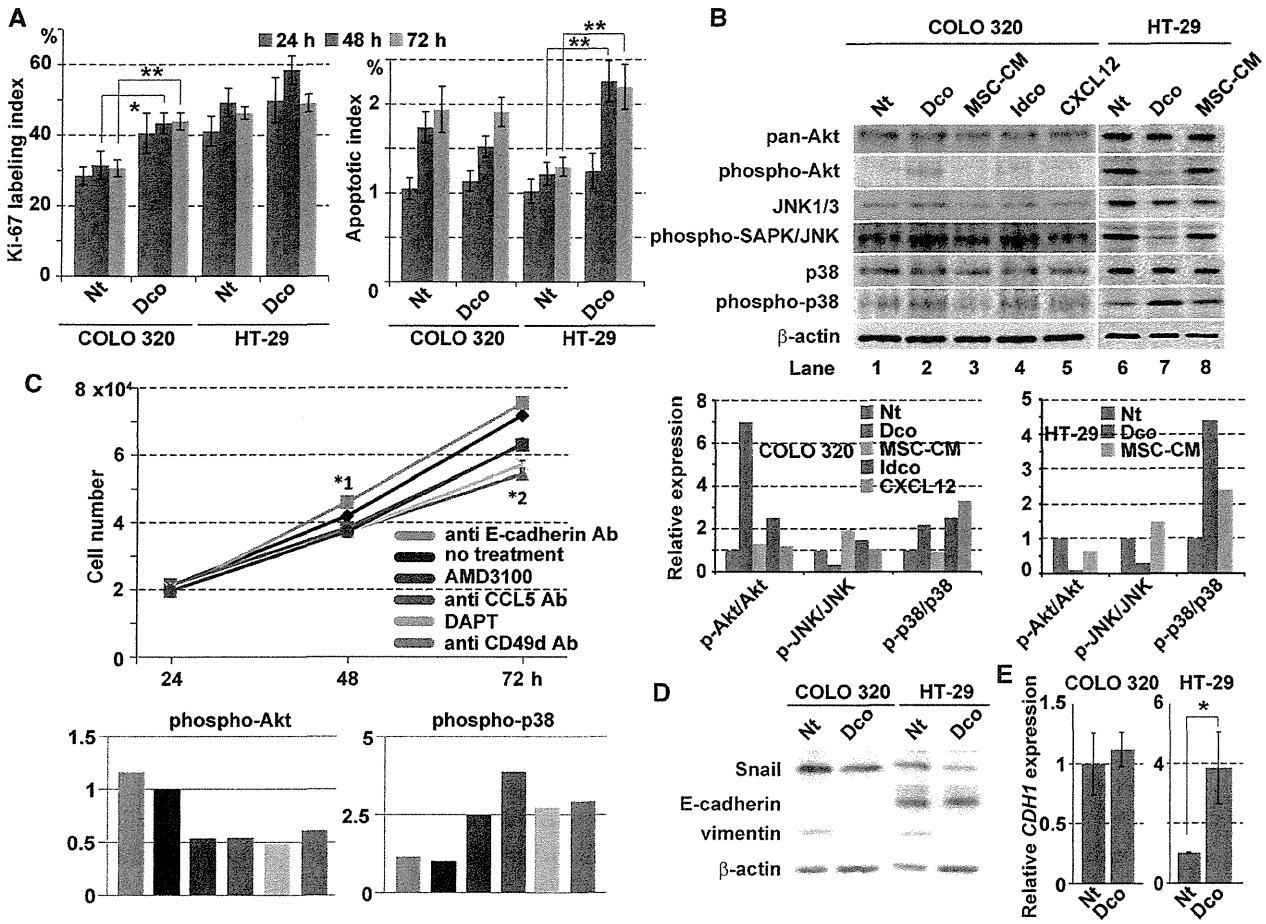

Fig. 5 Heterotypic interactions between rat MSCs as a cancer cell niche and human colon cancer cell lines. In direct co-culture with MSCs, cancer cells were separated by FACS based on GFP fluorescence. Transwell assays were used for the indirect co-culture procedure. COLO 320 and HT-29 cells were treated with MSC-CM, and COLO 320 cells were treated with recombinant CXCL12. **a** The Ki-67 labeling index and apoptotic index calculated from TUNEL staining are shown. **b** Western blot analysis was conducted on COLO-320 and HT-29 cells cultured alone or co-cultured with MSCs and probed for the proteins shown. Data are representative of three independent experiments. Phosphorylated protein expression relative to that in untreated cells for each of the three signaling pathways was quantified in comparison to the band intensity of unphosphorylated proteins in COLO-320 (*lower left panel*) and HT-29 (*lower right panel*) cells treated as indicated. **c** Proliferation of COLO 320 cells was assessed by the cell number counted by FACS under co-culture with rat MSCs for each anti-neutralizing antibody against human E-cadherin, CCL5, and CD49d (α4 integrin), or small molecule inhibitor of the CXCL12 receptor CXCR4, AMD3100, and γ-secretase inhibitor, DAPT. Proliferation of co-cultured COLO 320 cells under no treatments was a control designated as COLO 320 (co). Phosphorylated AKT (*lower left panel*) and p38 (*lower right panel*) protein expression relative to that in untreated COLO 320 cells for each of the five signaling pathways was quantified in comparison to the band intensity in Western blot analysis (see Supplementary Fig. 2b) of unphosphorylated proteins in COLO 320 cells treated as indicated in **c**. Western blot analysis of EMT signaling molecules (**d**) and qRT-PCR analysis of *CDH1* transcripts (**e**) in direct co-culture. *Nt* no treatment, *Dco* direct co-culture, *CDH1* E-cadherin, *CXCL12* chemokine (C-X-C motif) ligand 12, *CXCR4* chemokine (C-X-C motif) receptor 4, *Ccl5* chemokine (C–C motif) ligand 5, *CCR5* chemokine (C–C motif) receptor 5, *Jag1* Jagged 1, *Vcam1* vascular cell adhesion molecule-1, *Itga4* integrin α4. *Asterisks* indicate statistical significance: co-cultured MSCs significantly increased the Ki-67 labeling index of COLO 320 cells both at 48 h ($P = 0.044$) and 72 h ($P = 0.004$), while there was an increased apoptotic index of HT-29 cells at both 48 h ($P = 0.002$) and 72 h ($P = 0.006$, **a**). **c** *1, E-cadherin vs. CD49d $P = 0.001$, E-cadherin vs. CCL5 $P = 0.002$, E-cadherin vs. DAPT $P = 4.8E{-}4$; *2, E-cadherin vs. CD49d $P = 1.0E{-}6$, E-cadherin vs. CCL5 $P = 1.1E{-}4$, E-cadherin vs. DAPT $P = 2.0E{-}6$, E-cadherin vs. AMD3100 $P = 1.3E{-}4$, control vs. CD49d $P = 3.0E{-}6$, control vs. CCL5 $P = 0.003$, control vs. DAPT $P = 2.0E{-}5$, control vs. AMD3100 $P = 0.004$, CD49d vs. CCL5 $P = 0.003$, CD49d vs. AMD3100 $P = 1.3E{-}4$. **e** $P = 0.047$

subtly enhanced by blocking homotypic E-cadherin adhesion, whereas it was suppressed by a CXCR4 antagonist (AMD3100), Ccl5 neutralization, γ-secretase inhibition (DAPT), or CD49d blockage. The major ligand of vascular cell adhesion molecule-1 (Vcam-1) is integrin α4β1 (very late antigen-4, VLA-4), which is a dimer and composed of CD49d (α4) and CD29 (β1) (Fig. 5c, Supplementary Fig. 2b). Similarly, HT-29 cell proliferation was only